TITLE

Functional brain networks and neuroanatomy underpinning nausea severity can predict nausea susceptibility using machine learning

Short Title/RUNNING HEAD

Neuroimaging of nausea

Authors

Dr James K Ruffle* (1), Miss Anya Patel* (1), Dr Vincent Giampietro (2), Dr Matthew A Howard (2), Professor Gareth Sanger (1), Professor Paul L R Andrews (3), Professor Steven C R Williams (2), *Professor Qasim Aziz (1), *Dr Adam D Farmer (1,4,5)

1. Centre for Neuroscience and Trauma, Blizard Institute, Wingate Institute of Neurogastroenterology, Barts and the London School of Medicine & Dentistry, Queen Mary University of London, 26 Ashfield Street, London, E1 2AJ, UK
2. Department of Neuroimaging, King's College London, Institute of Psychiatry, Psychology & Neuroscience, London, SE5 8AF, UK
3. Division of Biomedical Sciences, St George's University of London, London, SW17 0RE, UK
4. Institute of Applied Clinical Sciences, University of Keele, Keele, ST5 5BG, UK

This is an Accepted Article that has been peer-reviewed and approved for publication in the The Journal of Physiology, but has yet to undergo copy-editing and proof correction. Please cite this article as an 'Accepted Article'; doi: 10.1113/JP277474.

5. Department of Gastroenterology, University Hospitals of North Midlands NHS Trust, Stoke on Trent, ST6 8QG, UK

** joint first authors*

** joint senior authors*

Address for Correspondence

Professor Qasim Aziz PhD FRCP

The Wingate Institute of Neurogastroenterology, Barts and the London School of Medicine and Dentistry, 26 Ashfield Street, Whitechapel, London, E1 2AJ, UK,

Tel: +44 (0)20 7882 2650, Fax: +44 (0)20 7375 2103, Email: q.aziz@qmul.ac.uk

Word Counts

Abstract 247

Total Manuscript 4000

Additional information

James Ruffle, Anya Patel, Adam D Farmer: acquisition of data; manuscript preparation; statistical analysis; study supervision; critical revision of the manuscript for important intellectual content.

Vincent Giampietro, Matthew A Howard: Acquisition of data; critical revision of the manuscript for important intellectual content.

Gareth Sanger, Paul Andrews, Steven C R Williams, Qasim Aziz: Pioneered study concept and design, technical or material support; obtained funding as principal applicant; critical revision of the manuscript for important intellectual content, project supervision.

None of the authors have any conflict of interests to declare.

These studies were funded by an NC3Rs project grant (ref - G0900797).

This work was presented as an oral abstract at the Federation of Neurogastroenterology and Motility, Amsterdam, 2018. The work was supported by a grant to QA from National Centre for Replacement, Refinement and Reduction of Animals in Research (NC3Rs), UK.

Abstract

OBJECTIVES: Nausea is a highly individual and variable experience. The central processing of nausea remains poorly understood, although numerous influential factors have been proposed including brain structure, function and autonomic nervous system (ANS) activity. We investigated the role of these factors in nausea severity and if susceptibility to nausea could be predicted using machine learning.

DESIGN: 28 healthy participants (15 male; mean age 24 years) underwent quantification of resting sympathetic and parasympathetic nervous system activity. All were exposed to a 10-minute motion-sickness video during fMRI. Neuroanatomical shape differences of the subcortex and functional brain networks associated with the severity of nausea were investigated. A machine learning neural network was trained to predict nausea susceptibility, or resistance, using baseline ANS data and detected brain features.

RESULTS: Increasing nausea scores positively correlated with shape variation of the left amygdala, right caudate and bilateral putamen (*corrected-p*=0.05). A functional brain network active in participants reporting nausea was identified implicating the thalamus, anterior, middle and posterior cingulate cortices, caudate nucleus and nucleus accumbens (*corrected-p*=0.043). Both neuroanatomical differences and the functional nausea-brain network were closely related to sympathetic nervous system activity. Using these data, a machine learning model predicted susceptibility to nausea with an overall accuracy of 82.1%.

CONCLUSIONS: Nausea severity relates to underlying subcortical morphology and a functional brain network in its experience; both measures are potential biomarkers in trials of anti-nausea therapies. The use of machine learning should be further investigated as an objective means to develop models predicting nausea susceptibility.

Key POINTS

- Nausea is an adverse experience characterised by alterations in autonomic and cerebral function. Susceptibility to nausea is difficult to predict, but machine learning has yet to be applied to this field of study.
- The severity of nausea that individuals experience is related to the underlying morphology (shape) of the subcortex; namely of the amygdala, caudate and putamen. A functional brain network related to nausea severity was identified, which included the thalamus, cingulate cortices (anterior, mid and posterior), caudate nucleus and nucleus accumbens. Sympathetic nervous system function and sympathovagal balance was closely related to both this nausea-associated anatomical variation and functional connectivity network. Machine learning accurately predicted susceptibility or resistance to nausea.
- These novel anatomical and functional brain biomarkers for nausea severity may permit objective identification of individuals susceptible to nausea, using artificial intelligence/machine learning. Brain data may be useful to identify individuals more susceptible to nausea.

Introduction

Nausea is an unpleasant experience that can precede vomiting and is amongst the most common and distressing gastrointestinal (GI) symptoms. The causes of nausea are diverse and include intrinsic gastroenterological disorders, motion sickness and pregnancy, and it is a frequent side effect of medications including chemotherapeutic and anaesthetic agents (Shupak & Gordon, 2006). Nausea has a population prevalence of 14% reported in a community based survey (Haug *et al.*, 2002). Although nausea is a common clinical symptom, anti-emetics have limited efficacy against nausea and treatments targeted specifically against nausea, irrespective of cause, are lacking (Sanger & Andrews, 2018).

There is marked intra and inter-individual variability in both susceptibility to nausea and the severity that individuals experience. Indeed, a number of factors have been proposed to influence an individual's experience of nausea, including demographics, autonomic nervous system (ANS) activity, and brain processing (Stern *et al.*, 2011b). Converging evidence suggests that the experience of nausea involves bidirectional interactions within the brain-gut-axis involving the central nervous system (CNS), autonomic nervous system, gastrointestinal physiology (including dysrhythmia) and endocrine pathways (Muth, 2006; Napadow *et al.*, 2013a; Napadow *et al.*, 2013b; Andrews & Sanger, 2014; Angeli *et al.*, 2015; Farmer *et al.*, 2015).

The lack of understanding of the central mechanisms of nausea is partially a consequence of the inherent challenges of studying it, given that animal models are significantly limited in their translational potential of a subjective and interoceptive human experience (Andrews & Sanger, 2014; Aziz & Ruffle, 2018). In human experimentation, nausea can be physiologically induced as a consequence of motion sickness, either by actual motion (Coriolis–cross-coupled stimulus; (Miller & Graybiel, 1970)) or through illusory self-motion, an epiphenomenon referred to as 'vection' (Koch, 1999). Nausea stimulated by vection is a form of visually induced motion sickness (VIMS), similar to true motion sickness insofar that it induces nausea and, at its most intense level, vomiting (Muth, 2006; Shupak & Gordon, 2006; Kennedy *et al.*, 2010).

Current understanding of the CNS changes that accompany the development and severity of nausea that individuals experience remains limited. Although functional neuroimaging techniques have been applied to the study of nausea (Napadow *et al.*, 2013b; Farmer *et al.*, 2015; Toschi *et al.*, 2017), they remain relatively scarce in comparison to those evaluating other aspects of GI sensation, such as visceral pain (Ruffle *et al.*, 2017). In previous studies utilising functional magnetic resonance imaging (fMRI), researchers variably demonstrated nausea-related activation of a number of brain areas salient to interoception such as the amygdala, putamen, pons, locus coerulus, and others associated with fear conditioning, such as the anterior insula and middle cingulate (Napadow *et al.*, 2013b; Farmer *et al.*, 2015; Sclocco *et al.*, 2016; Toschi *et al.*, 2017). Furthermore, neuroanatomical differences in white matter tracts have also been associated with increased nausea susceptibility

(Napadow *et al.*, 2013a). However, whilst certainly providing some insight into CNS mechanisms, existing studies are limited and have largely focused on the identification of singular brain regions involved in nausea (Farmer *et al.*, 2015), or pairwise connectivity between two areas (Toschi *et al.*, 2017). Given the complexity of the sensation of nausea, it seems likely that the physiological and interoceptive components of a nauseous experience are a result of many brain areas interacting in synchrony. To date, there remains minimal understanding of such networks in association with nausea. In addition, it is unknown whether patient stratification into those with and without nausea susceptibility can be achieved using machine learning based on these aforementioned brain differences.

Thus, the aims of the present study were threefold. *Firstly,* given that some individuals are significantly more susceptible to nausea than others, we hypothesised that this could be attributed to differences in the brain structure engendering the central autonomic network (Critchley & Harrison, 2013). We therefore we investigated subcortical brain morphological differences in individuals of varying sensitivities to nausea induced by visually-induced motion sickness. *Secondly*, we hypothesised that the complex experience of nausea is processed by multiple brain regions interacting synchronously as a functional network, which we aimed to probe with network-based statistics. *Thirdly*, as a proof of concept, we investigated whether patient stratification into those susceptible and resistant to nausea can be accurately predicted by artificial intelligence/machine learning (*see* (Russell & Norvig, 2009; Dey, 2016; Ruffle *et al.*, 2018d)), using brain (neuroanatomical and functional connectomic) and ANS data alone.

MaterialS AND Methods

Ethical Approval

All protocols were approved by King's College London Research Ethics Committee (*ref: PNM/09/09-04*). Written informed consent was obtained in all participants, and all studies conformed to the standards set by the latest revision of the Declaration of Helsinki. All participants were naïve to the experimental protocols.

Study population

28 healthy participants (15 male), aged 18-65 years, who had no known past medical history and were not currently taking any prescribed or over the counter medications, took part in the study. All were non-smokers and were asked to avoid caffeine and alcohol for 24 hours prior to the study. Females of child bearing potential were studied in the follicular stage of their menstrual cycle. The validated Hospital Anxiety and Depression Scale was used to screen for sub-clinical anxiety and depression (Zigmond & Snaith, 1983). All participants were right handed, as screened by the Edinburgh Handedness Inventory (Oldfield, 1971). Participants were studied in the afternoon (between 14:00-16:00) in a temperature-controlled thermoneutral (20-22°C) environment. Aspects of the experimental data have been published previously by our group (Farmer *et al.*, 2015), though for entirely disparate analytical investigations which are not reported in this manuscript.

Induction of nausea

We utilised a previously validated visual stimulus (Farmer *et al.*, 2015), a 10-minute video of a landscape (London Eye, Houses of Parliament) as seen from a point 2-metres above the centre of Westminster Bridge, London, UK. The video was composed with a sequence of digital camera images taken from the viewpoint of a tall subject standing on the bridge. The point of view rotated, panning the scene through 360-degrees at a rate of 0.2 Hz about an axis tilted 18-degrees from earth vertical. The tilted and rotated visual display instigates the perception of spinning on the spot about a tilted axis due to vection. Viewing a moving tilted scene has been shown to enhance the onset of visually induced motion sickness (Bubka & Bonato, 2003). A similar stimulus has previously been used to induce visually induced motion sickness (Golding *et al.*, 2012), and in our own laboratory produced an effective nauseogenic stimulus with this same paradigm (Farmer *et al.*, 2015). For fMRI, participants wore a pair of MR-compatible goggles (CinemaVision, Salvadorini Consulting LLC, Lexington, NC, USA) and were positioned supine in the MRI scanner. The goggles were used to project the motion video to the participant during scanning, allowing an unimpeded view of the stimulus. During the active scanning phase, the 10-minute motion video was projected through the goggles. Throughout the study, participants were instructed to remain still and to focus on the

stimulus as much as possible. On a separate day of scanning, participants underwent a second MRI wherein they viewed a static single image of this 10-minute video, which was used as a control to statistically compare to. Whether a participant would view the control or the motion video first was pseudorandomised.

During the motion video, experience of nausea was assessed using a 4-point visual analogue scale (VAS), where 1 represented no symptoms and a score of 4 represented severe nausea. The validated motion sickness sensitivity score (MSSQ) (Golding, 1998) and motion sickness assessment questionnaire (MSAQ) (Gianaros *et al.*, 2001) were used to assess susceptibility to and symptoms associated with motion sickness, respectively. The MSSQ questionnaire asks participants to rate their previous experiences of nausea as a child, and over the last 10 years, across 9 different situations, such as in a car, on a bus, on a train etc., scored on a 5-point Likert scale ranging from not applicable to frequently felt sick (Golding, 1998). The MSAQ evaluates the experience of motion sickness across GI, central, peripheral and sopite-related dimensions by asking participants to rate their sickness using a 9-point scale across 16 items (Gianaros *et al.*, 2001).

Autonomic measures by heart rate variability

Resting autonomic parameters were derived by virtue of heart rate variability (HRV) measures, in accordance with international recommendations (European *et al.*, 1996). In a quiet thermoneutral laboratory environment (to prevent MR scanner-related confounds), ECG electrodes (Ambu Blue Sensor P, Denmark) were placed at the cardiac apex, left and right sub-clavicular areas of each participant for ECG signal acquisition. ECG readings were digitally recorded using a bio-signals acquisition system (Neuroscope, Medifit Instruments, Enfield, Essex, UK) at 5 kHz. Resting autonomic activity was derived by validated non-invasive HRV cardiometrics; parasympathetic nervous system (PNS) activity by putative measure of efferent brainstem cardiac vagal tone (CVT) and sympathetic nervous system (SNS) activity by cardiac sympathetic index (CSI) (Julu, 1992; Toichi *et al.*, 1997). Sympathovagal balance were also approximated by the ratio between CSI [sympathetic] and CVT [parasympathetic]. After attachment of all autonomic recording apparatus, data were recorded for 5-minutes with participants asked to relax (but not fall asleep), during which *resting* autonomic tone

was derived. We have previously used this same method of quantifying resting autonomic measures for application to MRI data (see (Ruffle *et al.*, 2018b; Ruffle *et al.*, 2018c).

Parasympathetic Nervous System: Derivation of Resting Cardiac Vagal Tone

The derivation of resting parasympathetic activity by CVT is described in detail elsewhere (Farmer *et al.*, 2014). In brief, the incoming QRS complex is compared to a unique template, generated from the initial ECG acquisition stages of the individual. If the QRS complexes are sufficiently comparable, voltage gated oscillators within the Neuroscope generate a 1 mV pulse, which feeds to a two-limb circuit, consisting of a high-pass and low-pass limb. The high-pass limb precisely follows the incoming QRS signal, whilst the low-pass limb produces a damped rendition (Little *et al.*, 1999). Therefore, the lesser the delta change of an incoming signal, that is to say the lower the heart rate variability (HRV), the closer the low-pass limb will mimic that to the high-pass, resulting in a lower value. In contrast, the greater the HRV the more the low-pass limb will deviate from its high-pass counterpart, resulting in a higher value. This phenomenon is referred to as 'phase shift demodulation' and is uniquely based upon non-invasive measures of PNS tone. CVT is measured on a linear vagal scale (LVS), where a value of 0 is derived from fully atropinized healthy human volunteers (Julu & Hondo, 1992; Farmer *et al.*, 2014). Moreover, mathematically CVT correlates closely to other putative 'parasympathetic' measures, including both HRV and root mean square of successive differences (RMSSD) (Brock *et al.*, 2017).

Sympathetic Nervous System: Cardiac Sympathetic Index

Resting sympathetic nervous system (SNS) activity was quantified by means of the cardiac sympathetic index (CSI). To determine CSI, R-R interval data was first extracted from the ECG and manually reviewed to remove any artefacts. Subsequently, R-R data was transferred to the cardiac metric program, which yields a calculation of the validated Toichi's cardiac sympathetic index by use of the Lorenz plot (Toichi *et al.*, 1997). Notably, CSI is disparate to low frequency (LF) band analysis of HRV, and illustrated as superior to LF in ascertaining sympathetic function by (Toichi et al., 1997). CSI is expressed is a numerical ratio of R-R intervals and thus has no units (Farmer et al., 2013).

MRI acquisition

MRI data (T2*-weighted images) were collected on a General Electric Signa Excite II 1.5 Tesla HD scanner located at the Centre for Neuroimaging Sciences, Institute of Psychiatry, Psychology & Neuroscience, King's College London. Head movement was minimised by application of foam padding within the head coil and an eye movement tracker was mounted onto the head coil. For each participant, structural brain data were acquired via a high resolution T1-weighted 3D FSPGR structural scan, in sagittal orientation, using the following parameters: repetition time (TR) 7.02 ms; echo time (TE) 2.82 ms; inversion time (TI) 450 ms; slice thickness 1.1 mm; field of view 280 mm; flip angle 208; spatial positions 196; image matrix 256 x 256 x 196 voxels; in plane voxel dimensions 1.1 x 1.1 x 1.1 mm. During fMRI, 300 T2*-weighted images per slice (40 x 3 mm slices, 0.3 interslice gap, TE 25ms, TR 3500 ms, flip angle 90 degrees, matrix 64^2), depicting blood oxygen level dependent (BOLD) contrast, were collected as participants viewed the motion video.

Pre-processing of structural MRI data

Raw structural MRI images were first carefully manually reviewed to check for signal and image artefacts that may otherwise confound findings. Subsequently, subcortical structural pre-processing (for analysis of morphology/shape) was conducted using FSL-FIRST 5.0, an algorithm that uses Bayesian statistics for automated brain segmentation (Patenaude *et al.*, 2011). This approach identifies and segments each anatomical scan into 15 subcortical regions: bilateral nucleus accumbens, amygdala, caudate, hippocampus, pallidum, putamen and thalamus, plus the brainstem. All scans were registered to 1mm standard space (Montreal Neurological Institute (MNI) 152), to account for overall differences in the shape and size of each subject's skull and brain. The 15 subcortical nuclei regions of interest (ROI) were registered to subcortical ROI templates and segmented. Both registrations (whole scan and ROI) were manually checked for correct template-scan alignment. All segmentations were manually reviewed for error prior to analytical use. Each resultant subcortical nuclei were concatenated to a single 4D structural file (1 volume per subject) to permit statistical analysis. Additionally, volumetric data, in mm^3, were also extracted from these regions for *post-hoc* machine learning feature synthesis (*see later)*. All statistical analysis of structural MR data was undertaken with general linear modelling (GLM) against nausea VAS scores,

wherein demeaned demographical covariates, age and gender, were included as nuisance regressors.

Pre-processing of functional MRI data

fMRI data pre-processing was undertaken using FMRI Expert Analysis Tool (FEAT) version 5.98, part of the FMRIB Software Library (FSL) software package (www.fmrib.ox.ac.uk/fsl) (Smith *et al.*, 2004). The following pre-statistics processing was applied; Motion Correction with FMRIB Linear Image Registration Tool (MCFLIRT) (7 degrees of freedom); slice-timing correction using Fourier-space time-series phase-shifting; brain extraction (BET); spatial smoothing using a Gaussian kernel of full-width-half-maximum (FWHM) 5mm; grand-mean intensity normalisation of the entire 4-dimensional dataset by a single multiplicative factor; high pass temporal filtering (Gaussian-weighted least-squares straight line fitting, with sigma=50.0s). Registration to high resolution structural and standard space images was carried out using the FMRIB Linear Image Registration Tool (FLIRT).

Network-Based Statistics

Using *a priori* selection of regions (Stern *et al.*, 2011a; Napadow *et al.*, 2012; Critchley & Harrison, 2013), 22 regions of interest (ROI) parcellation masks were generated using the Harvard-Oxford Cortical Structural Probability Atlas and FSLeyes (Smith *et al.*, 2004), to identify regions for functional activity data to be extracted from. Masks were thresholded to a maximal region probability of ≥ 65%, binarised, and aligned to their specific anatomical areas on each individual's scan. The 22 functional ROIs included 14 of the aforementioned structurally-segmented subcortical ROIs: bilateral nucleus accumbens, amygdala, caudate, hippocampus, pallidum, putamen and thalamus. Furthermore, the hypothalamus, bilateral insula, bilateral orbitofrontal cortex and anterior (ACC), middle (MCC) and posterior cingulate cortices (PCC) were added. Within FSLeyes, the Talairach brain map was used to delineate the hypothalamus as presently no Harvard map exists for this region (Talairach & Tournoux, 1988); this approach is in keeping with previous fMRI studies investigating this brain structure (Baroncini *et al.*, 2012). Brainstem sub-regions were *omitted* from the network-based

analysis as we felt it questionable if the tesla strength of the scanner would permit stringent analysis of such small brainstem nuclei (such as the nucleus tractus solitarii). The inclusion of ROIs in investigating for a role in the brain processing of nausea was also cross-referenced with NeuroSynth to provide insight to any possible confounds of the data (such as additional roles of the brain regions, for example in visual processing) (Yarkoni *et al.*, 2011). Using MATLAB (version 2018a, uk.mathworks.com), BOLD signal from each ROI, or '*node'*, was cross-correlated, producing correlation matrices of 55 node-node connective correlation (*r)* values, or '*edges'* (resultant of binomial coefficient $\left(\frac{22}{2}\right) = 231;$ or 22 "$choose$" 2). Our specific aim was to investigate functional connectivity between these areas and thus did not statistically test activity of singular regions (such as the ACC). The rationale for this is because previous findings of brain activity to nauseogenic stimuli are already reported elsewhere, including with this experimental paradigm (Farmer *et al.*, 2015).

The Network Based Statistics (NBS) connectome toolbox (version 1.2 https://www.nitrc.org/projects/nbs/) was used to investigate brain network differences contingent on the severity of nausea experienced during the motion video (Zalesky *et al.*, 2010). The NBS is a non-parametric statistical method which corrects for multiple comparisons, and controls for the family-wise error rate (FWER). The NBS is the graph analogue of cluster-based statistical methods used in mass univariate testing on all voxels in an image and produces clusters in topological space (as opposed to physical space). NBS relies on permutation testing (Freedman & Lane method (Freedman & Lane, 1983)) to determine significance within general linear modelling (GLM), which includes regression of nuisance predictors, permuting resulting residuals and subsequently adding permuted residuals back to nuisance signal to give a realisation of data under the null hypothesis. This approach recognizes that permuting raw data is not desirable as it may engender some variability explained by nuisance predictors. It is rather the error terms that can be permuted and estimated under the null hypothesis as a part of the data not explained by the nuisance regressors; that is, the residuals (Anderson & Robinson, 2008). The method permits derivation of FWER-corrected *p*-values using permutation testing when investigating brain networks with fMRI (Sporns *et al.*, 2005). The performed NBS analyses were linear contrasts of nausea VAS scores by GLM (with demeaned demographical nuisance covariates added), using 10,000 permutations and the criteria

for significance set to FWER-corrected $p < 0.05$. Motion video analyses were also statistically compared to the control period to limit for an attention or gaze-driven confound. A primary edge parameter threshold of 2.64 was used to accommodate for a Cohen's *d* medium-effect size of 0.5 (Zalesky *et al.*, 2010). Results were visualized using the BrainNet illustrative package (http://www.nitrc.org/projects/bnv/) (Xia *et al.*, 2013).

Analysis of demographic and psychophysiological data

Autonomic, demographic and psychophysiological data normality distributions were tested using the Shapiro-Wilk normality test. $P<0.05$ was adopted as the criterion to indicate statistical significance. Parametric statistical analyses of autonomic, nausea VAS and relationship to neuroimaging data found (including network properties) were performed using MATLAB (version 2018a, uk.mathworks.com), IBM SPSS Statistics (IBM Corp. Released 2017. IBM SPSS Statistics for Windows, Version 25.0. Armonk, NY: IBM Corp) and GraphPad Prism (version 6.00, GraphPad Software, La Jolla California, USA, www.graphpad.com).

Machine Learning – Neural Network Development

A machine learning approach was used as a *post-hoc* proof of concept (Ruffle *et al.*, 2018d). Our principal aim was to establish if susceptibility or resistance to nausea (by virtue of VIMS) could be accurately predicted from neuro-quantitative data. This was undertaken using the MATLAB statistics and machine learning toolbox, with a shallow neural network and scaled conjugate gradient backpropagation learning. Predictive features for the model were neuroanatomical, connectivity, and autonomic (both parasympathetic and sympathetic) in nature, determined from aforementioned analyses undertaken. Additional feature synthesis was undertaken by determining subcortical volumetric symmetry ratios. The response target to be predicted by the model was susceptibility or resistance to nausea, which was binarised so that a minimum VAS score of 1 was equivalent to nausea-resistance (0) and VAS scores >1 indicated nausea-susceptibility (+1). Five neurons were allocated to the hidden layer of the machine learning's neural network. Model hidden layer processing included sigmoid positive transfer function and sigmoid symmetric transfer function

steps. Data were partitioned randomly to 70% for model training, 15% for model validation and the final 15% for model testing, as per conventional standard (Russell & Norvig, 2009; Dey, 2016). Model validation were undertaken with cross-entropy as per default toolbox settings.

RESULTS

MSSQ score is a poor predictor of nausea severity

MSSQ (susceptibility to motion sickness by recollection of previous experiences) was not significantly correlated with either VAS or MSAQ (MSSQ and VAS: r=0.34, p=0.08; MSSQ and MSAQ: r=0.25, p=0.20) (Supplementary Figure S1), indicative that the MSSQ is a poor predictive scoring system for determining nausea severity; at least in this sample and in response to this stimulus.

Resting sympathetic nervous system activity, by cardiac sympathetic index, relates to the severity of nausea experienced

Severity of nausea experienced (VAS) during fMRI was significantly positively correlated to resting CSI [sympathetic tone] (r=0.43, p=0.023) (Figure 1A). Resting CVT [parasympathetic] did not significantly correlate to the nausea VAS (r=-0.32 p=0.095) (Figure 1B). CSI/CVT ratio [sympathovagal balance] at rest was significantly positively correlated to severity of nausea experienced (r=0.42, p=0.026) (Figure 1C).

[Insert Figure 1]

Subcortical shape, but not volume, differs according to severity of nausea experienced

Vertex (shape) analysis showed that morphological differences of the left amygdala, right caudate and bilateral putamen linearly were significantly related to *increasing* nausea severity (threshold free cluster enhancement ([TFCE]-corrected p=0.05 (Figure 2, Supplementary Video S1). There were

no significant variations in morphology [shape] associated with *decreasing* nausea severity. There were no significant correlations between raw subcortical structure volumes and nausea VAS.

[Insert Figure 2]

Nausea-related shape of the subcortex is sympathetically-related by cardiac sympathetic index

In *post-hoc* analyses, we sought to investigate if these nausea-related morphological changes could be partially related to the HRV measures of autonomic nervous system (Ruffle *et al.*, 2018b). In particular, we repeated GLM with alternate regression control for CVT [parasympathetic] and CSI [sympathetic]. Interestingly, these aforementioned morphological changes of the subcortex remained significant, despite nuisance covariate regression for CVT. However, with regression for CSI, the shape changes of the left amygdala, putamen and right caudate became non-significant, while the right putamen did remain significant. This suggests that these nausea-related neuroanatomical differences could closely align to CSI [sympathetic] function.

A functional brain network relates to nausea severity

A significant functional brain network was identified that positively correlated with nausea severity (FWER-corrected p=0.043) (Figure 3). When thresholded to a Cohen's d of 0.5 (medium effect size), this network comprised 7 nodes with 7 functional connections ('edges') (Figure 3A) (Supplementary Video S1). Brain regions implicated were: ACC, MCC, PCC, left and right thalamus; right caudate and right nucleus accumbens. Significant edges (functional connections) of this network were the following: PCC-MCC; left thalamus-MCC; right thalamus-MCC; left thalamus-ACC; MCC-right caudate; MCC-nucleus accumbens and ACC-right Caudate. Edge strengths defined as the degree of relationship in nausea severity to functional connectivity are listed in Figure 3B & C. In comparison, there was no significant functional network identified when viewing the control video (p=1.00).

[Insert Figure 3]

Brain networks of nausea severity relate to resting autonomic measures of heart rate variability

Relationships between nausea network connectivity CSI [sympathetic], CVT [parasympathetic] and CSI / CVT ratio [sympathovagal balance] were investigated further. We found a highly significant (albeit weak) positive correlation between total network connectivity and resting CSI (r=0.24, p=0.0008) as well as CSI / CVT ratio (r=0.21, p=0.003). A correlation between network connectivity and resting CVT was not apparent (r=-0.13, p=0.07). In exploratory post-hoc analyses, a machine learning stepwise linear model built a weak, albeit significant, linear model of resting CSI, using this nausea-related network connectivity data (F 4.60, p=0.04). Furthermore, individual functional connections of the brain network and their relation to autonomic measures of HRV are available in the supplementary material (Supplementary Figure 2-4).

Machine learning predicts susceptibility to nausea from brain and autonomic data: proof of concept

A predictive model for binary susceptibly to nausea (i.e. susceptible *vs*. resistant) was developed by virtue of a shallow neural network (Ruffle *et al.*, 2018d). Predictive inputs to the neural network comprised aforementioned functional connectivity, neuroanatomical data and resting HRV measures of the ANS. (Figure 4A). The model was trained on 70% of data (partitioned by random data division), which trained to an accuracy of 80% (area under curve (AUC) 0.80) (Figure 4B). When testing the model with the remaining unseen data, it accurately allocated an individual to the nausea-resistant or susceptible category with an accuracy of 100% (AUC 1.00) (Figure 4C). The total accuracy for all data, irrespective of data partition, was 82.1% (AUC 0.82) (Figure 4D-E). Total true positive (TPR) and false negative rate (FNR) for nausea susceptibility was 100% and 0%, respectively. TPR and FNR for nausea resistance was 58.3% and 41.7%, respectively. Total Positive predictive value (PPV) for nausea susceptibility was 76.2% (false discovery rate (FDR) for nausea resistance = 23.8%), whilst negative predictive value (NPV) for nausea resistance was 100% (FDR for nausea susceptibility = 0%).

[Insert Figure 4]

DISCUSSION

Nausea is a complex and troublesome symptom and its central brain mechanisms remain incompletely characterised. This study builds upon contemporaneous research and adds the following novel findings: i) identification of a relationship between underlying subcortical neuroanatomy and nausea severity, ii) delineation of a novel functional brain network relating to severity of nausea experienced, iii) interrelationships between nausea severity, autonomic neurophysiology, brain structure and connectivity, and iv) how coalescence of these findings can be used to predict susceptibility to nausea by artificial intelligence/machine learning, as a proof of concept. We elaborate on these four key findings below.

A neuroanatomical predisposition to nausea

An individual's cross sensitivity to differing nausea stimuli exhibits similarity, meaning that if an individual was sensitive to a given nauseogenic stimulus, such as motion-sickness, they are typically sensitive to other nauseogenic stimuli, such as chemotherapy induced nausea and vomiting (Golding, 1998). We reason that this predictability in an individual's sensitivity to nauseogenic stimuli could be partially attributed to their underlying neuroanatomy. Here, we specifically focussed on the sub-cortex as of its interplay to the central autonomic network (Critchley & Harrison, 2013; Aziz & Ruffle, 2018). To that end, we identified four subcortical nuclei displaying variation in their shape (or 'morphology') dependent on *increasing* nausea i.e. the left amygdala, right caudate and bilateral putamen. Notably, the amygdala has a key role in the central autonomic network (Benarroch, 1993), and the involvement of basal ganglia regions in a sympathetic-related stress response is in keeping with our previous findings from separate studies/datasets (Borsook *et al.*, 2010; Ruffle *et al.*, 2018b).

Nausea-related subcortical morphology may be sympathetically-related

The association of these particular subcortical nuclei to nausea severity is intriguing, given that in a separate group of individuals we have previously shown that these nuclei vary in shape or volume

depending on either resting sympathetic or parasympathetic tone (see (Ruffle *et al.*, 2018b)). Additionally, the notion that the basal ganglia and amygdala have a regulatory function in ANS physiology has been previously described (Pazo *et al.*, 1981; Nalivaiko & Blessing, 2001; Blessing, 2003). It is somewhat expected therefore that in repeating this analysis with controlled-regression of each participant's sympathetic tone, which we would posit is pro-nauseogenic (Farmer *et al.*, 2015; Kenward *et al.*, 2015; Singh *et al.*, 2016), these anatomical areas became almost entirely non-significant.

A novel functional brain network relates to severity of nausea experienced

We identified a novel network of functional connectivity, which represents the extent of information transmission and synchrony between multiple brain regions whilst exposed to a nauseous stimulus. In the processing of an inherently complex interoceptive phenomenon such as nausea, it seems highly likely that this percept is a result of multiple areas of the brain interacting at a given time. As such, this study aims to build upon previous studies of brain activity or connectivity between two brain regions only (Farmer *et al.*, 2015; Toschi *et al.*, 2017). In particular, we identified a network which increased in strength (functional connectivity / information transfer) in line with increasing nausea severity, which encompassed the anterior, mid and posterior cingulate cortices, both sides of the thalamus, right caudate nucleus and nucleus accumbens. Some of these regions have known associations to nausea (Napadow *et al.*, 2013b; Farmer *et al.*, 2015; Sclocco *et al.*, 2016; Toschi *et al.*, 2017), although their co-relationship to autonomic neurophysiology seems salient and will be elaborated on below.

The identified brain network of nausea severity was related to autonomic neurophysiology

Notably, the connectivity of the identified nausea-severity network correlated positively with both sympathetic nervous system tone and sympathovagal balance. As already stipulated above, given a presupposition of increased/elevated sympathetic tone as pro-nauseogenic (Farmer *et al.*, 2015; Kenward *et al.*, 2015; Singh *et al.*, 2016), it is interesting to also find a concomitant autonomic association to this network, wherein greater connectivity corresponded both to greater nausea

severity and sympathetic tone. We have already discussed some of these brain regions and their known role in autonomic regulation, though in this network we additionally implicate the thalamus, cingulate cortex and accumbens, all of which are known to have a role in sympathetic neuro-regulation, or a sympathetic response to events meriting emotional arousal (such as nausea or pain) (Critchley & Harrison, 2013; Ruffle *et al.*, 2018a; Ruffle *et al.*, 2018b). Hence, it is reasonable to suggest that this neural network reflects SNS-related nausea processing. Future work should investigate if a trilinear relationship between this functional brain network, autonomic measures and GI measures (such as with electrogastrogram or self-reported epigastric symptoms) exist in real-time synchrony. It would be prudent to also investigate additional nauseogenic stimuli in this context, including non-visual, to ensure no confound from visual processing / saccades (though our data here was compared to a control visual stimulus). Furthermore, investigation with measures of attention and arousal would be useful for future study to examine relation of these to the findings.

Artificial intelligence to predict nausea susceptibility

Lastly, as a proof of concept, we illustrate how complex neurophysiological data, such as functional connectivity, neuroanatomy and autonomic neurophysiology can be coalesced with machine learning to build a model in order to predict sensitivity or resistance to nausea, induced by VIMS. In the last few years, interest in machine learning has increased exponentially, and its application to academia and healthcare is rapidly developing (Ruffle *et al.*, 2018d). However, the use of this technology in predicting difficult or 'softer' endpoints, such as subjective reporting of nausea, presents an intriguing clinical opportunity. It should be noted however that this model aimed to reflect a proof of concept *only* and limitations do exist, namely that a larger sample size and disparate nausea stimuli would be required to further develop such a network for either future academic work or for deployment in a healthcare setting. That being said, this proof of concept model alone led to a high level of accuracy, raising the question of whether machine learning with such brain data could be used to predict susceptibility to unpleasant experiences, such as nausea and visceral pain.

Conclusions

In this study, we build on previous studies investigating brain activity related to nausea and illustrate the brain processing of nausea as a functional network. To our knowledge, this is the first study using network analysis to describe how multiple brain regions communicate to give rise to the perception of nausea. The study is also the first to investigate the interrelationship between subcortical morphology and predisposition to nausea experience, not least by demonstrating its close-knit relationship to autonomic neurophysiology (Ruffle *et al.*, 2018b). Finally, as a proof of concept, we illustrated how a given individual's underlying neuroanatomy, functional connectivity and autonomic neurophysiology can be coalesced to predict susceptibility or resistance to nausea, using a novel machine learning approach. Future work should interrogate the use of machine learning to predict nausea susceptibility (including from multiple nauseogenic stimuli), be it from brain data, autonomic or otherwise to determine if the described brain functional connectivity parameters could act as biomarkers to study the efficacy of novel nausea therapies.

REFERENCES

Anderson MJ & Robinson J. (2008). Permutation Tests for Linear Models. *Australian & New Zealand Journal of Statistics* **43,** 75-88.

Andrews PL & Sanger GJ. (2014). Nausea and the quest for the perfect anti-emetic. *European journal of pharmacology* **722,** 108-121.

Angeli TR, Cheng LK, Du P, Wang TH, Bernard CE, Vannucchi MG, Faussone-Pellegrini MS, Lahr C, Vather R, Windsor JA, Farrugia G, Abell TL & O'Grady G. (2015). Loss of Interstitial Cells of Cajal and Patterns of Gastric Dysrhythmia in Patients With Chronic Unexplained Nausea and Vomiting. *Gastroenterology* **149,** 56-66 e55.

Aziz Q & Ruffle JK. (2018). The neurobiology of gut feelings. In *The interoceptive basis of the mind*, ed. Tsakiris M & De Preester H, pp. 1-46. Oxford University Press.

Baroncini M, Jissendi P, Balland E, Besson P, Pruvo JP, Francke JP, Dewailly D, Blond S & Prevot V. (2012). MRI atlas of the human hypothalamus. *Neuroimage* **59,** 168-180.

Benarroch EE. (1993). The central autonomic network: functional organization, dysfunction, and perspective. *Mayo Clinic proceedings* **68,** 988-1001.

Blessing WW. (2003). Lower brainstem pathways regulating sympathetically mediated changes in cutaneous blood flow. *Cell Mol Neurobiol* **23,** 527-538.

Borsook D, Upadhyay J, Chudler EH & Becerra L. (2010). A key role of the basal ganglia in pain and analgesia--insights gained through human functional imaging. *Mol Pain* **6,** 27.

Brock C, Jessen N, Brock B, Jakobsen PE, Hansen TK, Rantanen JM, Riahi S, Dimitrova YK, Dons-Jensen A, Aziz Q, Drewes AM & Farmer AD. (2017). Cardiac vagal tone, a non-invasive measure of parasympathetic tone, is a clinically relevant tool in Type 1 diabetes mellitus. *Diabet Med*.

Bubka A & Bonato F. (2003). Optokinetic drum tilt hastens the onset of vection-induced motion sickness. *Aviation, space, and environmental medicine* **74,** 315-319.

Critchley HD & Harrison NA. (2013). Visceral influences on brain and behavior. *Neuron* **77,** 624-638.

Dey A. (2016). Machine Learning Algorithms: A Review. *IJCSIT* **7,** 1174-1179.

European, Society, of & Cardiology. (1996). Heart rate variability: standards of measurement, physiological interpretation and clinical use. Task Force of the European Society of Cardiology and the North American Society of Pacing and Electrophysiology. *Circulation* **93,** 1043-1065.

Farmer AD, Ban VF, Coen SJ, Sanger GJ, Barker GJ, Gresty MA, Giampietro VP, Williams SC, Webb DL, Hellstrom PM, Andrews PL & Aziz Q. (2015). Visually induced nausea causes characteristic changes in cerebral, autonomic and endocrine function in humans. *The Journal of physiology* **593,** 1183-1196.

Farmer AD, Coen SJ, Kano M, Weltens N, Ly HG, Botha C, Paine PA, Oudenhove LV & Aziz Q. (2014). Normal values and reproducibility of the real-time index of vagal tone in healthy humans: a multi-center study. *Annals of gastroenterology : quarterly publication of the Hellenic Society of Gastroenterology* **27,** 362-368.

Farmer AD, Coen SJ, Kano M, Worthen SF, Rossiter HE, Navqi H, Scott SM, Furlong PL & Aziz Q. (2013). Psychological traits influence autonomic nervous system recovery following esophageal intubation in health and functional chest pain. *Neurogastroenterol Motil* **25,** 950-e772.

Freedman D & Lane D. (1983). A Nonstochastic Interpretation of Reported Significance Levels. *Journal of Business & Economic Statistics* **1,** 292-298.

Gianaros PJ, Muth ER, Mordkoff JT, Levine ME & Stern RM. (2001). A questionnaire for the assessment of the multiple dimensions of motion sickness. *Aviation, space, and environmental medicine* **72,** 115-119.

Golding JF. (1998). Motion sickness susceptibility questionnaire revised and its relationship to other forms of sickness. *Brain research bulletin* **47,** 507-516.

Golding JF, Doolan K, Acharya A, Tribak M & Gresty MA. (2012). Cognitive cues and visually induced motion sickness. *Aviation, space, and environmental medicine* **83,** 477-482.

Haug TT, Mykletun A & Dahl AA. (2002). The prevalence of nausea in the community: psychological, social and somatic factors. *Gen Hosp Psychiatry* **24,** 81-86.

Julu PO. (1992). A linear scale for measuring vagal tone in man. *Journal of autonomic pharmacology* **12,** 109-115.

Julu PO & Hondo RG. (1992). Effects of atropine on autonomic indices based on electrocardiographic R-R intervals in healthy volunteers. *Journal of neurology, neurosurgery, and psychiatry* **55,** 31-35.

Kennedy RS, Drexler J & Kennedy RC. (2010). Research in visually induced motion sickness. *Applied ergonomics* **41,** 494-503.

Kenward H, Pelligand L, Savary-Bataille K & Elliott J. (2015). Nausea: current knowledge of mechanisms, measurement and clinical impact. *Vet J* **203,** 36-43.

Koch KL. (1999). Illusory self-motion and motion sickness: a model for brain-gut interactions and nausea. *Digestive diseases and sciences* **44,** 53S-57S.

Little CJ, Julu PO, Hansen S & Reid SW. (1999). Real-time measurement of cardiac vagal tone in conscious dogs. *The American journal of physiology* **276,** H758-765.

Miller EF, 2nd & Graybiel A. (1970). A provocative test for grading susceptibility to motion sickness yielding a single numerical score. *Acta oto-laryngologica Supplementum* **274,** 1-20.

Muth ER. (2006). Motion and space sickness: intestinal and autonomic correlates. *Auton Neurosci* **129,** 58-66.

Nalivaiko E & Blessing WW. (2001). Raphe region mediates changes in cutaneous vascular tone elicited by stimulation of amygdala and hypothalamus in rabbits. *Brain Res* **891,** 130-137.

Napadow V, Sheehan J, Kim J, Dassatti A, Thurler AH, Surjanhata B, Vangel M, Makris N, Schaechter JD & Kuo B. (2013a). Brain white matter microstructure is associated with susceptibility to motion-induced nausea. *Neurogastroenterol Motil* **25,** 448-450, e303.

Napadow V, Sheehan JD, Kim J, Lacount LT, Park K, Kaptchuk TJ, Rosen BR & Kuo B. (2012). The brain circuitry underlying the temporal evolution of nausea in humans. *Cereb Cortex* **23,** 806-813.

Napadow V, Sheehan JD, Kim J, Lacount LT, Park K, Kaptchuk TJ, Rosen BR & Kuo B. (2013b). The brain circuitry underlying the temporal evolution of nausea in humans. *Cereb Cortex* **23,** 806-813.

Oldfield RC. (1971). The assessment and analysis of handedness: the Edinburgh inventory. *Neuropsychologia* **9,** 97-113.

Patenaude B, Smith SM, Kennedy DN & Jenkinson M. (2011). A Bayesian model of shape and appearance for subcortical brain segmentation. *Neuroimage* **56,** 907-922.

Pazo JH, Tumilasci OR & Medina JH. (1981). Studies on the mechanisms of L-dopa-induced salivary secretion. *European journal of pharmacology* **69,** 255-261.

Ruffle JK, Aziz Q & Farmer AD. (2018a). Pro-nociceptive effects mediated by adenosinergic A2A activity at the nucleus accumbens; but what about the autonomic nervous system? *Pain* **159,** 997.

Ruffle JK, Coen SJ, Giampietro V, Williams SCR, Apkarian AV, Farmer AD & Aziz Q. (2018b). Morphology of subcortical brain nuclei is associated with autonomic function in healthy humans. *Hum Brain Mapp* **39,** 381-392.

Ruffle JK, Coen SJ, Giampietro V, Williams SCR, Aziz Q & Farmer AD. (2018c). Preliminary report: parasympathetic tone links to functional brain networks during the anticipation and experience of visceral pain. *Scientific reports* **8,** 13410.

Ruffle JK, Farmer AD & Aziz Q. (2018d). Artificial Intelligence Assisted Gastroenterology - Promises and Pitfalls. *Am J Gastroenterol* ***ePub ahead of print.***

Ruffle JK, Frokjaer JB & Farmer AD. (2017). Neuroimaging of Visceral Pain. In *Neuroimaging of Pain*, ed. Saba L, pp. 341-374. Springer International Publishing, Cham.

Russell SJ & Norvig P. (2009). *Artificial Inteliigence, A Modern Approach*. Pearson Education.

Sanger GJ & Andrews PLR. (2018). A History of Drug Discovery for Treatment of Nausea and Vomiting and the Implications for Future Research. *Front Pharmacol* **9,** 913.

Sclocco R, Kim J, Garcia RG, Sheehan JD, Beissner F, Bianchi AM, Cerutti S, Kuo B, Barbieri R & Napadow V. (2016). Brain Circuitry Supporting Multi-Organ Autonomic Outflow in Response to Nausea. *Cereb Cortex* **26,** 485-497.

Shupak A & Gordon CR. (2006). Motion sickness: advances in pathogenesis, prediction, prevention, and treatment. *Aviation, space, and environmental medicine* **77,** 1213-1223.

Singh P, Yoon SS & Kuo B. (2016). Nausea: a review of pathophysiology and therapeutics. *Therap Adv Gastroenterol* **9,** 98-112.

Smith SM, Jenkinson M, Woolrich MW, Beckmann CF, Behrens TE, Johansen-Berg H, Bannister PR, De Luca M, Drobnjak I, Flitney DE, Niazy RK, Saunders J, Vickers J, Zhang Y, De Stefano N, Brady JM & Matthews PM. (2004). Advances in functional and structural MR image analysis and implementation as FSL. *Neuroimage* **23 Suppl 1,** S208-219.

Sporns O, Tononi G & Kötter R. (2005). The Human Connectome: A Structural Description of the Human Brain. *PLOS Computational Biology* **1,** e42.

Stern R, Koch K & Andrews P. (2011a). *Nausea: mechanisms and management.* University Oxford Press., New York.

Stern RM, Koch KL & Andrews PLR. (2011b). *Nausea : mechanisms and management*. Oxford University Press, New York.

Talairach J & Tournoux P. (1988). Co-Planar Stereotaxic Atlas of the Human Brain: 3-D Proportional System: An Approach to Cerebral Imaging: 3-Dimensional Proportional System: An Approach to Cerebral Imaging. 132.

Toichi M, Sugiura T, Murai T & Sengoku A. (1997). A new method of assessing cardiac autonomic function and its comparison with spectral analysis and coefficient of variation of R-R interval. *Journal of the autonomic nervous system* **62,** 79-84.

Toschi N, Kim J, Sclocco R, Duggento A, Barbieri R, Kuo B & Napadow V. (2017). Motion sickness increases functional connectivity between visual motion and nausea-associated brain regions. *Autonomic neuroscience : basic & clinical* **202,** 108-113.

Xia M, Wang J & He Y. (2013). BrainNet Viewer: a network visualization tool for human brain connectomics. *PLoS One* **8,** e68910.

Yarkoni T, Poldrack RA, Nichols TE, Van Essen DC & Wager TD. (2011). NeuroSynth: a new platform for large-scale automated synthesis of human functional neuroimaging data. *Frontiers in Neuroinformatics*.

Zalesky A, Fornito A & Bullmore ET. (2010). Network-based statistic: identifying differences in brain networks. *Neuroimage* **53,** 1197-1207.

Zigmond AS & Snaith RP. (1983). The hospital anxiety and depression scale. *Acta psychiatrica Scandinavica* **67,** 361-370.

AUTHOR BIOGRAPHY

Dr James K. Ruffle MBBS BSc is an Academic Clinical Fellow in clinical radiology at University College London Hospitals NHS Trust and honorary research fellow in neurogastroenterology at the Wingate Institute of Neurogastroenterology, Blizard Institute, Queen Mary University of London. His work involves the neurobiology of visceral sensations, including nausea and pain, including with the use of neuroimaging and data-science-driven techniques.

Miss Anya Patel BSc is medical student at the University of Birmingham. She undertook analysis of this data for her Neuroscience BSc project thesis at Barts and the London School of Medicine and Dentistry, Queen Mary University of London.

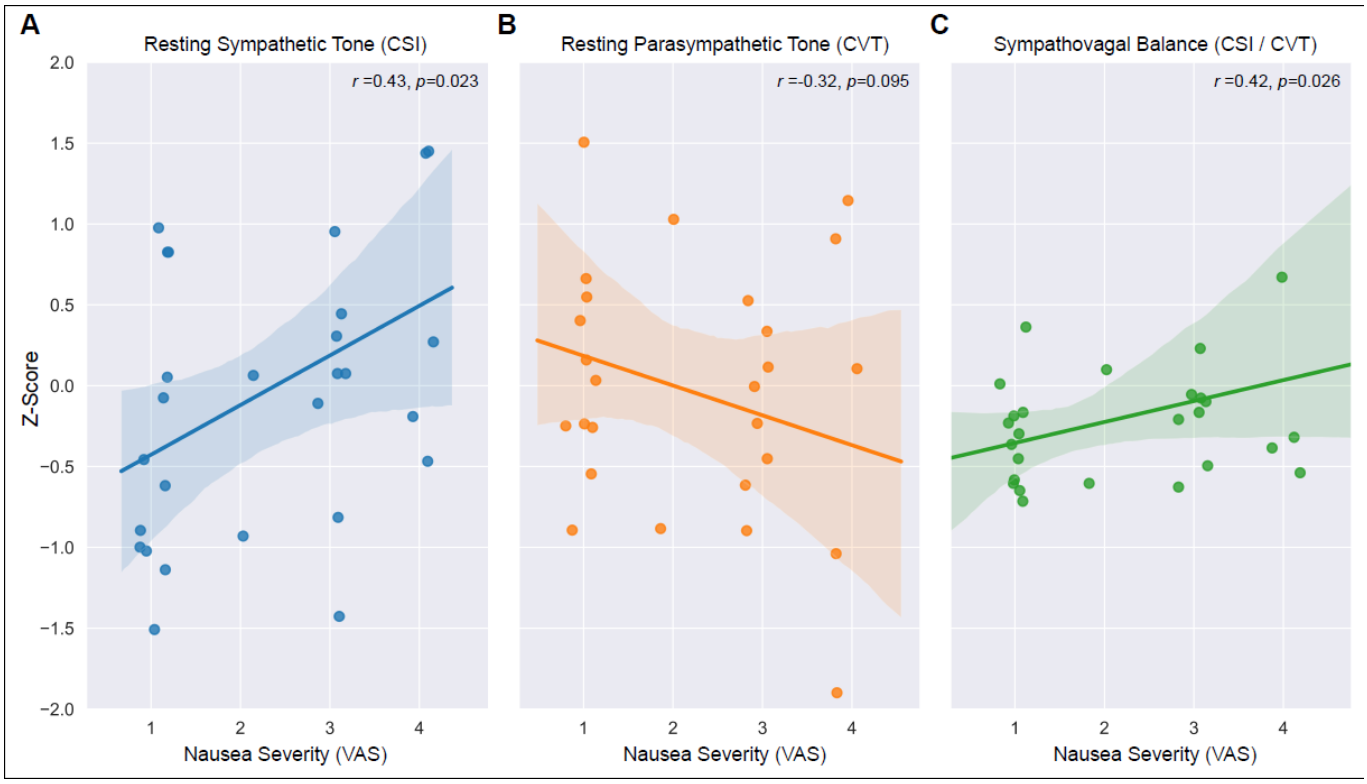

Figure 1 – Severity of nausea relates to resting autonomic nervous system function

Both resting sympathetic tone (A) and sympathovagal balance (C) are significantly positively correlated to nausea severity during scanning, whilst a non-significant negative correlative trend for resting parasympathetic tone was apparent (B). Data Z-scored for illustrative purposes. N=28. Line of best fit from linear regression with python robust outlier fitting, shaded area represents 95% confidence interval. Abbreviations: CSI, cardiac sympathetic index; CVT, cardiac vagal tone; VAS, visual analogue scale.

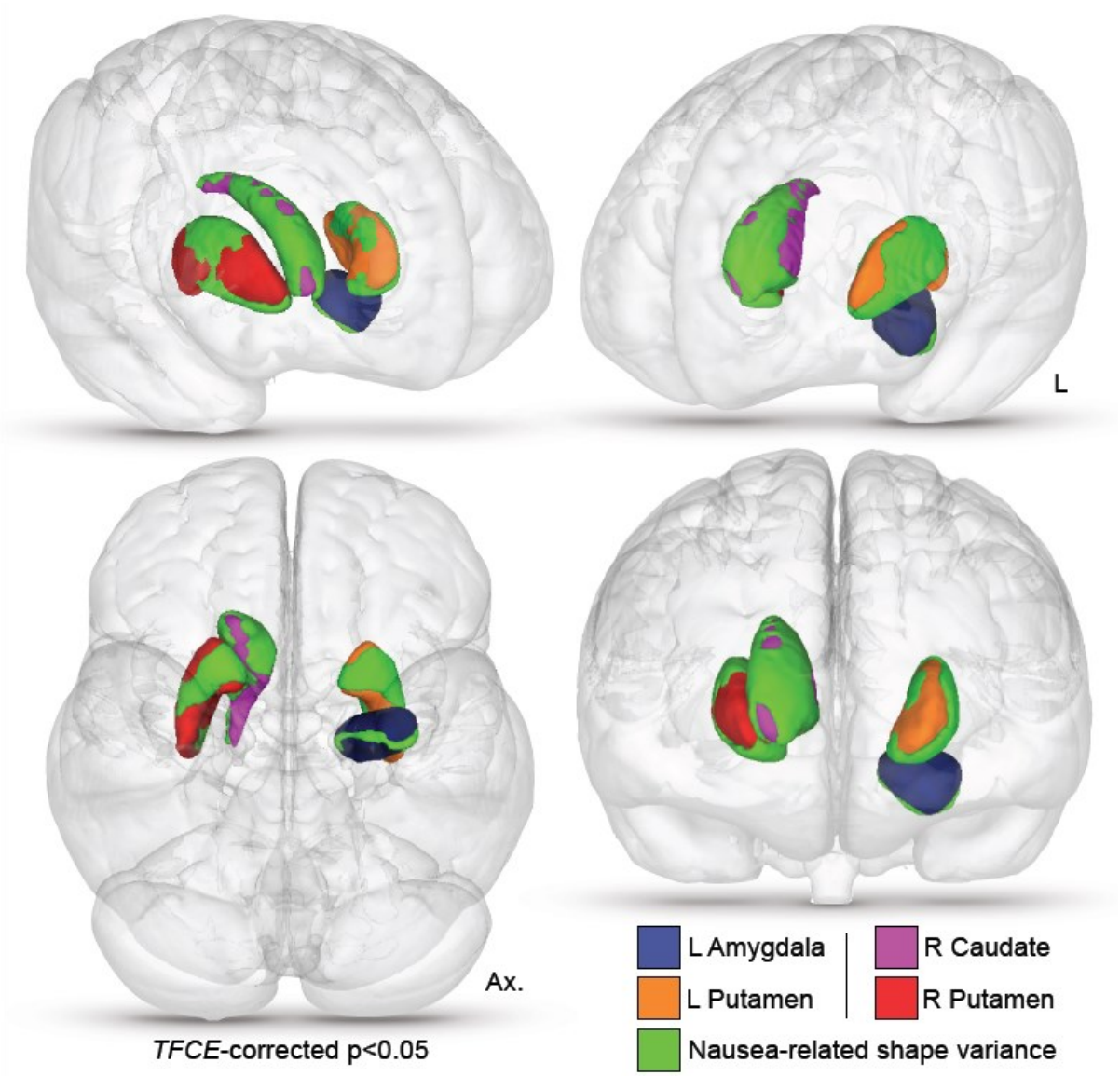

Figure 2 – Nausea-related subcortical shape variance

Vertex deformation (shape) variance which positively linearly related to increasing nausea severity. Subcortical masks colour-coded as per the given key, with overlaid aspects of nausea-related morphology. Statistical significance is TFCE-corrected and further thresholded to display only vertices of corrected-*p*<0.05. Abbreviations: Ax, axial. L, left; R, right; TFCE, threshold free cluster enhancement.

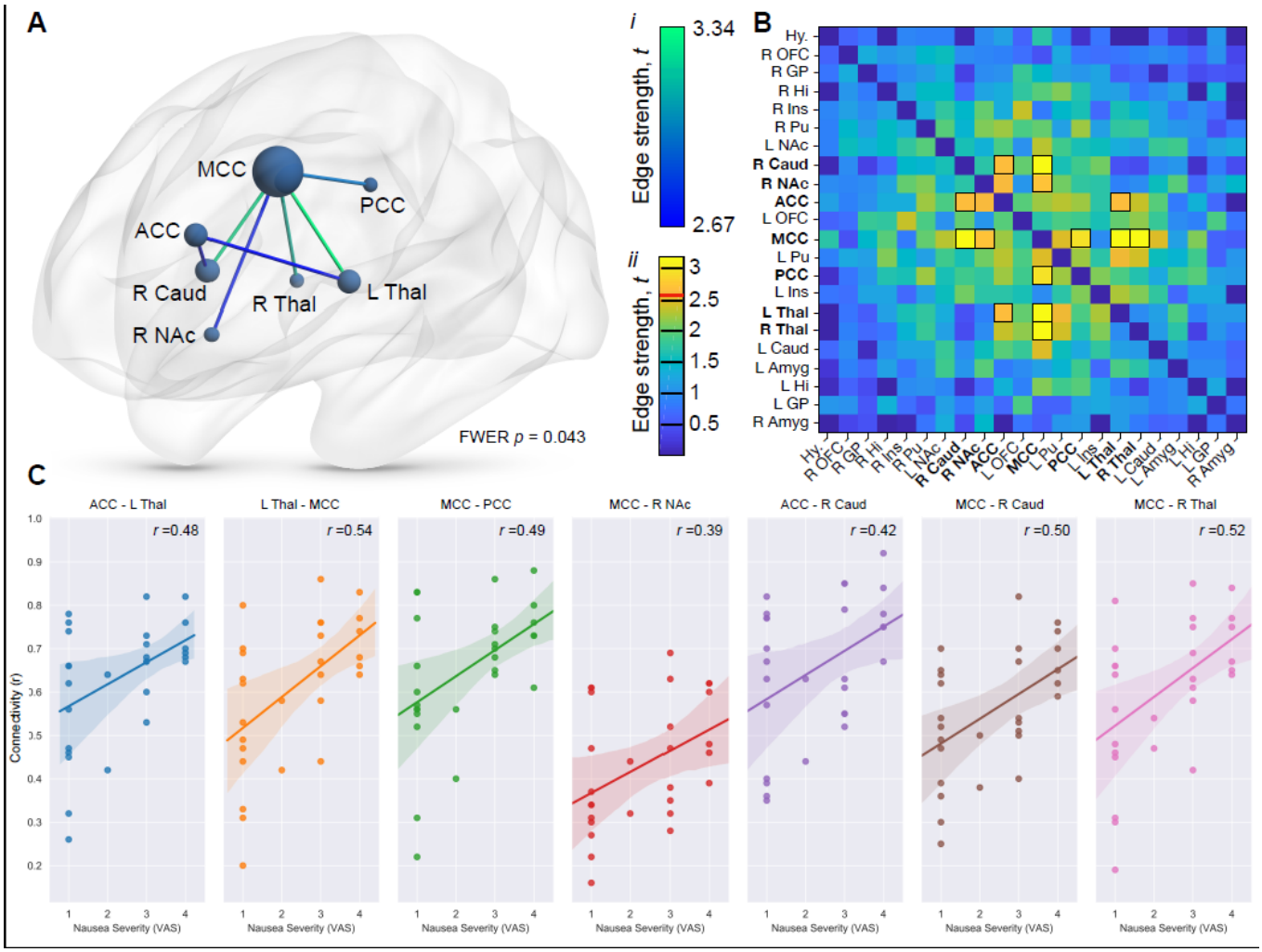

Figure 3 – A novel functional brain network related to nausea severity

A) Network-based statistics identified a significant functional brain network implicating 7 nodes of our *a priori* defined 22, all of which had edge strengths > 2.64, equivalent to a medium effect size Cohen's *d* of > 0.5. Nodes are sized according to their degree centrality (number of significant functional connections, or 'edges'). Edges are colour coded according to strength of effect size (see colour key, *i*). B) Edge-strength colour-map of all nodes tested with network-based statistics, wherein edges are colour coded according to strength of effect size (see colour key, *ii*, wherein a red line demarcates the critical edge-strength for inclusion in the functional network). Functional connections included in the network have been highlighted with black squares. C) Pairwise connectivity values (i.e. between a given 2 nodes) of the functional network, scatter-plotted against nausea severity (VAS). N=28. Line of best fit from linear regression with python robust outlier fitting, shaded area represents 95% confidence interval. Abbreviations: ACC, anterior cingulate cortex; Amyg, amygdala; Caud, caudate nucleus; FWER, family wise error rate; GP, globus pallidus (pallidum); Hi, hippocampus; Hy, hypothalamus; Ins, insula cortex; L, left; MCC, mid cingulate cortex; NAc, nucleus accumbens; OFC, orbitofrontal cortex; PCC, posterior cingulate cortex; Pu, putamen; R, right; Thal, thalamus; VAS, visual analogue score.

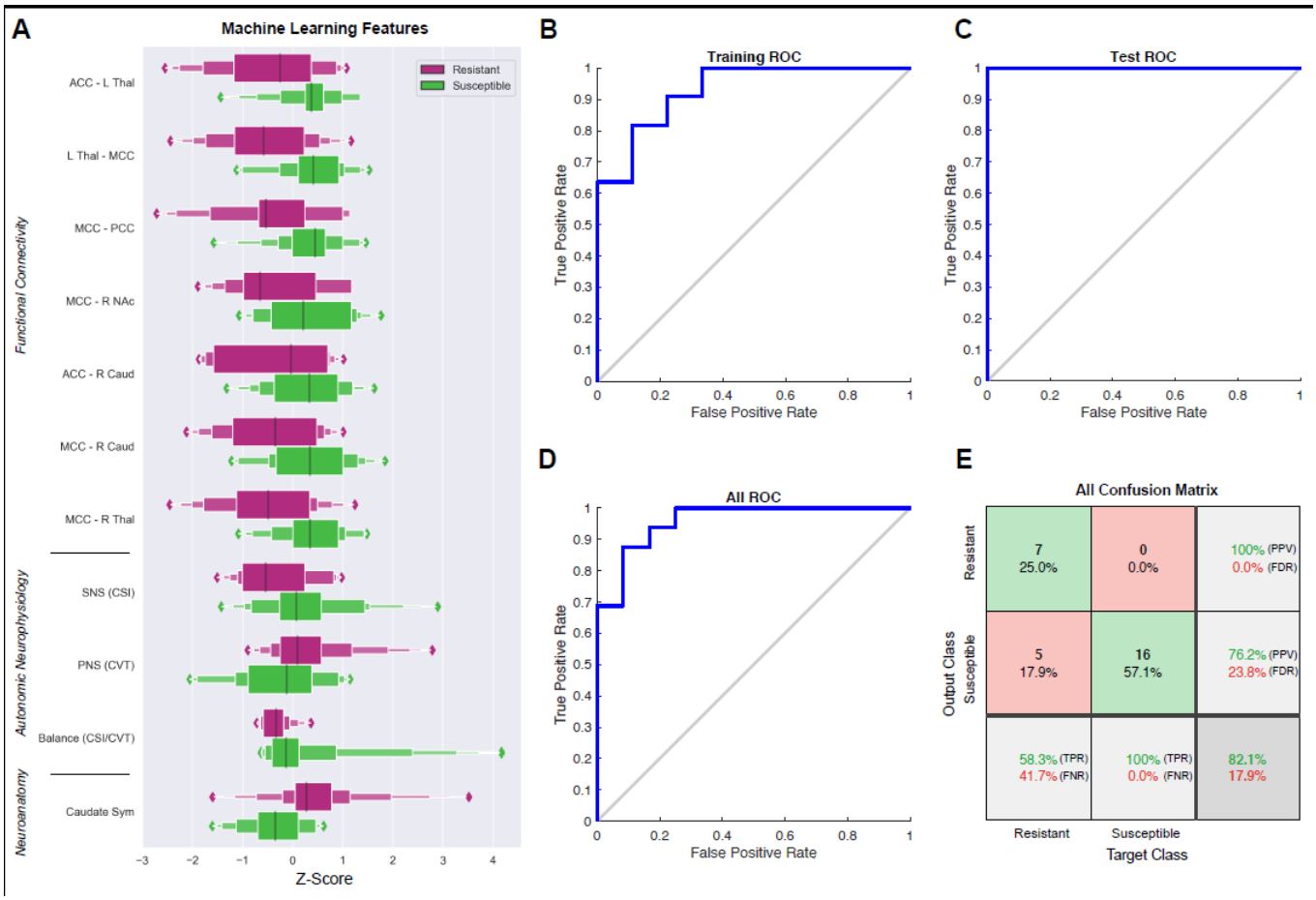

Figure 4 – Proof of concept: a machine learning neural network to predict susceptibility or resistance to nausea

A) A machine learning neural network was trained to predict susceptibility to nausea in the form of a binary classifier (i.e. susceptible or resistant). Eleven feature vectors were used in this model: 7 functional connections of the identified nausea network (see Figure 3), CVT, CSI, CSI/CVT ratio (see Figure 1) and caudate volumetric symmetry ratios, derived from further feature selection. Exponential boxplots illustrate the relationship of one feature to nausea resistance (purple) or susceptible (green), on a z-scored x axis. B) Receiver operator characteristic (ROC) curve of training state. The model was *trained* to an initial accuracy of 80% (AUC 0.80) with random data division, utilizing 70% of total samples. C) ROC curve of testing state. *Test* subsample (15%) correctly identified according to nausea susceptible at 100% accuracy. D) Total ROC for all data partitions (AUC 0.82). E) Confusion matrix for total predictive network properties. Abbreviations: ACC, anterior cingulate cortex; AUC, area under the curve; Caud, caudate nucleus; CSI, cardiac sympathetic index; CVT, cardiac vagal tone; FDR, false discovery rate; FNR, false negative rate; L, left; MCC, mid cingulate cortex; NAc, nucleus accumbens; PCC, posterior cingulate cortex; PPV, positive predictive value; R, right; ROC, receiver operator characteristic; Sym, symmetry; Thal, thalamus; TPR, true positive rate.